Inorganic Chemistry

Article

pubs.acs.org/IC

Self-Assembled Ln(III)$_4$ (Ln = Eu, Gd, Dy, Ho, Yb) [2 × 2] Square Grids: a New Class of Lanthanide Cluster

Nicholas M. Randell, Muhammad U. Anwar, Marcus W. Drover, Louise N. Dawe, and Laurence K. Thompson*

Department of Chemistry, Memorial University, St. John's, NL, A1B3X7, Canada

Supporting Information

ABSTRACT: Self-assembly of the Ln(III) ions (Ln = Eu, Gd, Dy, Ho, Yb) into square [2 × 2] grid-like arrays has been readily effected using simple, symmetric ditopic ligands based on a carbohydrazone core. The metal ions are connected via single atom bridges (e.g., μ_2-O$_{hydrazone}$, μ_2-OH, μ_2-OMe, μ_2-1,1-N_3^-, μ_4-O), depending on reaction conditions. The Gd(III)$_4$ examples exhibit intramolecular antiferromagnetic exchange ($-J < 0.11$ cm^{-1}), and in one Dy(III)$_4$ example, with a combination of μ_2-1,1-N_3^-, and μ_4-O bridges linking adjacent metal ions, SMM behavior is observed. One thermally driven relaxation process is observed in the temperature range 10−25 K ($\tau_0 = 6.5(1) \times 10^{-7}$ s, $U_{eff} = 110(1)$ K) in the presence of an 1800 Oe external field, employed to suppress a second quantum based relaxation process. The extended group of Ln(III) ions which submit to this controlled self-assembly, typical of the transition metal ions, indicates the general applicability of this approach to the lanthanides. This occurs despite the anticipated limitations based on larger ionic radii and coordination numbers, and is an encouraging sign for extension to larger grids with appropriately chosen polytopic ligands.

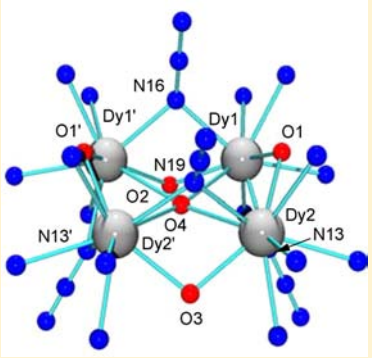

INTRODUCTION

Single molecule magnets (SMMs) have been a focus of intense interest since the discovery that the now classic Mn_{12} carboxylate clusters show slow magnetc relaxation as a result of a high spin ground state, and large single ion anisotropy, which occurs through noncompensation of total spin due to antiferromagnetic exchange between the high spin Mn(III) and Mn(IV) centers. It is the fortuitous alignment of the individual easy axes of the anisotropic metal centers which leads to the SMM behavior. However, blocking temperatures for systems of this sort remain low with values only as high as 5 K.[1−3] This low temperature limitation has been a challenge to synthetic chemists, and more recent attention has been focused on polymetallic lanthanide complexes, due in large measure to the significant single ion anisotropy inherent to most Ln(III) ions. Some Dy(III) systems have been shown to behave as SMMs, with examples of dinuclear, trinuclear, tetranuclear, and higher order clusters.[4−10] These clusters generally form from phenolic based ligands, which provide bridging interactions between lanthanide ions through short μ-O bridges, and lead to orientations of the individual lanthanide single ion anisotropy axes in some specific, but generally uncontrolled manner. Separating exchange effects in such systems from the dominant Ln(III) single ion properties is difficult, but it is becoming apparent that the net orientation of the anisotropy axes may in fact be the overriding factor in determining whether or not the cluster exhibits SMM behavior.[4,8,10]

We have recently begun to explore lanthanide complexation reactions of a number of poly *n*-topic hydrazone based ligands (*n* = 1−5; see Chart 1 for tritopic examples), which readily form self-assembled square [*n* × *n*] (*n* = 2−5) [M_4−M_{25} respectively; M from Mn, Fe, Co, Ni, Cu, Zn) polymetallic transition metal grid complexes in high yield.[11−13] Within the grids the metal ions are connected only by the hydrazone oxygen atoms, leading to a compact and regular arrangement of metal ions in close proximity (M-M distances ∼4 Å), and a preferred organization of their coordination spheres, and in most cases a specific alignment of their principal orbital axes.

The tritopic ligands have so far only produced mononuclear (2poap) and trinuclear (2pomp) Ln(III) derivatives.[14] The trinuclear (Ln(III)$_3$) complexes (Ln = La, Gd, Dy) have spiral bis-ligand double-stranded helicate structures, with each ligand pocket occupied by a Ln(III) ion. Interestingly SMM behavior is observed for the Dy_3 complex.[14] The metal ions reside in the tridentate ligand pockets, with the larger Ln(III) ions projecting from their respective ligand sites, seemingly inhibiting grid formation. For the Dy(III) complex the helical arrangement orients the metal ion coordination spheres in a slightly offset manner, which suggests a small mutual canting of their easy axes, which may be responsible for the SMM behavior.[14] This summation of effects of local magnetic axes has been considered in μ-O-phenoxy dinuclear Dy(III)$_2$[4] and triangular Dy(III)$_3$[8,10] complexes. In the Dy(III)$_3$ equilateral triangle case this led surprisingly to a nonmagnetic ground state, and intramolecular antiferromagnetic exchange. This was rationalized in terms of the axes lying in the plane of the triangle in a toroidal fashion.[10]

Received: April 9, 2013
Published: May 16, 2013

dx.doi.org/10.1021/ic4008813 | *Inorg. Chem.* 2013, 52, 6731−6742

Chart 1. Structural Representation of Some Polytopic Hydrazone Ligands

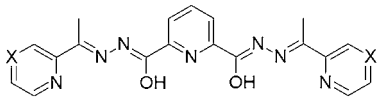

2poap (R=NH_2, X= CH), 2pomp (R= CH_3, X=CH)
2popp (R= Ph, X=CH), 2poapz (R=NH_2, X= N)

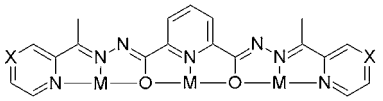

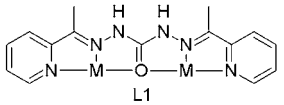

L1

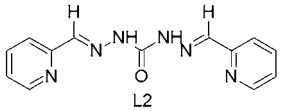

L2

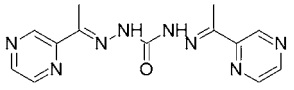

L3

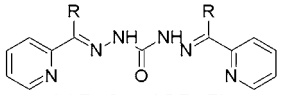

L4 R= 2-py, L5 R= Ph

The observation that the Ln(III) ions occupied all the 2pomp pockets in the trinuclear complexes, but not with 2poap, where just the central pocket was occupied, suggested that ligand flexibility might be an important feature in accommodating the Ln(III) ions. Therefore, other hydrazone based ligands were examined, with exocyclic Me groups (R) rather than NH_2. The analogous ditopic carbohydrazone ligand L1 (Chart 1), which readily forms square μ-O bridged [2 × 2] grids with, for example, Fe(II) and Co(II),[15] was examined. Reaction of L1 with $DyCl_3{\cdot}6H_2O$ and $Tb(NO_3)_3{\cdot}5H_2O$ in MeCN/MeOH in the absence or presence of NaN_3 successfully produced the first genuine examples of square, heteroleptic self-assembled [2 × 2] Ln(III)$_4$ grids $[Dy_4(L1\text{-}2H)_2(L1\text{-}H)_2(OH)_4]Cl_2{\cdot}8H_2O$, $[Dy_4(L1\text{-}2H)_2(L1\text{-}H)_2(N_3)_4(O)]{\cdot}14H_2O$, and $[Tb_4(L1\text{-}2H)(L1\text{-}H)_3(N_3)_4(O)](NO_3)(CH_3CN){\cdot}2H_2O$, in which the four Ln(III) ions are accommodated in exactly the same way as their transition metal ion counterparts, occupying the two tridentate ligand pockets in four ligands, arranged in pairs above and below the planar, square core arrangement of four Dy(III) and Tb(III) ions.[16] In both the Dy(III) and Tb(III) azide complexes the Ln(III) centers are bridged through μ_2-1,1 azide and μ_4-O (oxide) bridges. In the Dy(III) azide case SMM behavior was observed, with two clearly defined relaxation processes in both zero and applied fields (U_{eff} = 51 K ($\tau_0 = 3.0 \times 10^{-9}$ s) and U_{eff} = 91 K ($\tau_0 = 4.5 \times 10^{-7}$ s)) for the low and high temperature domains in zero field and with an optimum applied dc field (1600 Oe), which reduces quantum tunnelling of magnetization (QTM), the anisotropic energy barrier was calculated based on the maxima of the peaks and was found to be U_{eff} = 270 K ($\tau_0 = 4.0 \times 10^{-10}$ s). This represents a significant thermal barrier to magnetization reversal and indicates that grid arrangements of Dy(III) ions may have strong potential for tuning of such properties into a higher temperature regime. The Dy(III)(hydroxide) and Tb(III)(azide) [2 × 2] grids do not exhibit SMM behavior above 2 K, indicating that such behavior is specific to the Ln(III) ion, and also the presence of azide and oxide bridges.[16]

The present report expands the scope of this self-assembly approach to organized square [2 × 2] grid arrays of the Ln(III) ions, with other examples involving Gd(III) and Dy(III), including a new Dy(III) SMM, and new examples with Ho(III), Yb(III), Eu(III), involving a series of carbohydrazone ligands related to L1 (Chart 1). Structural and magnetic properties are discussed.

EXPERIMENTAL SECTION

Single Crystal X-ray Diffraction Studies. Crystals of **1**−**7** were mounted on low temperature diffraction loops and measured on a Rigaku Saturn CCD area detector with graphite monochromated Mo−Kα radiation, equipped with a SHINE optic. Structures were solved by direct methods (SHELXL[17] for **1**, and **4**−**7**, or SIR2004[18] for **2** and **3**) and expanded using Fourier techniques.[19] Neutral atom scattering factors were taken from Cromer and Waber.[20] Anomalous dispersion effects were included in Fcalc[21] the values for $\Delta f'$ and $\Delta f''$ were those of Creagh and McAuley.[22] The values for the mass attenuation coefficients are those of Creagh and Hubbell.[23] All calculations were performed using CrystalStructure[24,25] and Platon[26] crystallographic software packages, except for refinement, which was performed using SHELXL-97.[17] Non-hydrogen atoms were refined anisotropically, while hydrogen atoms were introduced in calculated positions and refined on a riding model, unless otherwise indicated. CCDC nos. 932666−932561. A summary of the refinement results is shown in Table 1.

For **3**, one of the bridging azide ligands was disordered over two orientations. Similarity restraints were applied to this molecule and to a half-occupancy lattice solvent acetonitrile molecule. O5−7 are lattice solvent water molecules for which the corresponding H-atoms could not be located from difference maps, but have been included in the formula for the calculation of intensive properties.

The Platon[26] SQUEEZE procedure was applied to **1**, **2**, and **4**−**7**. For **1**, 1033 electrons per unit cell were recovered in two voids that were sufficiently large to contain a small molecule (total volume 2536 Å^3); that is 258 electrons per formula unit. The two voids are considered to each contain 12 CH_3CN and 12 CH_3OH molecules (480 electrons; 6 CH_3CN and 6 CH_3OH molecules per formula unit). Similarity, distance, and angles restraints were applied to the uncoordinated pyridine rings. For **2**, 1021 electrons per unit cell were recovered in two voids that were sufficiently large to contain lattice solvent molecules (total volume 3549 Å^3); that is, 255.25 electrons per formula unit. Diffuse electron density was present prior to the application of SQUEEZE, and this has been assigned as two molecules of acetonitrile and 21 lattice solvent water molecules per formula unit. Similarity restraints were applied to one of the azide molecules in the model. For **5**, 484 electrons per unit cell were recovered in one void (total volume 1443 Å^3); that is, 242 electrons per formula unit. Diffuse electron density was present prior to the application of SQUEEZE, and was assigned as 19 lattice solvent H_2O and two CH_3CN molecules per formula unit. For **6**, 1102 electrons per unit cell were recovered in two voids that were sufficiently large to contain small molecules (total volume 4584 Å^3); that is, 137.75 electrons per formula unit. Lattice solvent water molecules were present, and the electrons recovered by SQUEEZE have been assigned as 13 water molecules per formula unit. For **7**, 524 electrons per unit cell were recovered in one void that was sufficiently large to contain lattice solvent molecules (total volume 1415 Å^3); that is, 262 electrons per formula unit. Diffuse electron density was present prior to the application of SQUEEZE, and this has been assigned as 26 H_2O molecules per formula unit. Similarity and isotropic restraints were applied to several of the atoms in the terminal ligand rings.

For **4**, difficulty was initially encountered in assigning a Laue class. The data appeared to be I-centered, tetragonal; however, this led to a "doubling" of the ligands (i.e., eight overlapping ligands per four metal centers). The data was reintegrated as P-centered, triclinic, leading to

dx.doi.org/10.1021/ic4008813 | Inorg. Chem. 2013, 52, 6731−6742

Table 1. Crystallographic Details for Complexes 1−7

	1	2	3	4
chemical Formula	$C_{114}H_{118}Gd_4N_{38}O_{14}$	$C_{56}H_{98}Gd_4N_{46}O_{26}$	$C_{55}H_{55.5}Cl_3Dy_4N_{37.5}O_8$	$C_{78}H_{122}Cl_2Dy_4N_{48}O_{30}$
M	2873.43	2460.68	2126.15	2933.03
T(K)	163(2)	168(2)	163(2)	163(2)
crystal system	monoclinic	orthorhombic	orthorhombic	triclinic
space group	$C2/c$ (#15)	$Pnna$ (#52)	$Cmc2_1$ (#36)	$P1$(#1)
a (Å)	16.307(12)	23.509(6)	17.511(5)	16.4445(14)
b (Å)	24.630(17)	20.041(5)	19.543(6)	16.4535(14)
c (Å)	27.68(2)	20.041(5)	22.117(6)	28.082(2)
α (deg)	90	90	90	76.921(5)
β (deg)	98.697(14)	90	90	76.941(5)
γ (deg)	90	90	90	62.389(4)
V (Å^3)	10 990(14)	9442(4)	7569(4)	6493.3(9)
Z	4	4	4	2
D_{calc} (g/cm^3)	1.737	1.731	1.866	1.500
μ(MoKα) (cm^{-1})	24.72	28.66	40.91	24.01
refs total	62722	76532	36191	57492
refs unique ($I > 2.00\sigma(I)$)	11381 (8249)	9688 (7443)	8934 (8737)	35655 (16755)
R_{int}	0.0855	0.0776	0.0394	0.0245
R_1 ($I > 2.00\sigma(I)$)	0.0892	0.0651	0.0317	0.0393
wR_2 (all reflections)	0.2650	0.1910	0.0846	0.1332

	5	6	7
chemical formula	$C_{69}H_{110}N_{42}O_{28}Yb_4$	$C_{60}H_{84}Eu_4N_{36}O_{18}$	$C_{65}H_{118}Ho_4N_{40}O_{35}$
M	2668.05	2205.39	2679.62
T(K)	123(2)	123(2)	163(2)
crystal system	triclinic	monoclinic	triclinic
space group	$P\bar{1}$ (#2)	$C2/c$ (#15)	$P\bar{1}$ (#2)
a (Å)	16.799(4)	41.38(2)	16.828(9)
b (Å)	17.177(5)	19.795(8)	17.240(12)
c (Å)	19.662(6)	27.676(14)	19.669(12)
α (deg)	80.722(17)	90	81.35(4)
β (deg)	69.340(15)	129.142(6)	69.31(3)
γ (deg)	67.267(15)	90	67.21(2)
V (Å^3)	4894(2)	17582(14)	4921(5)
Z	2	8	2
D_{calc} (g/cm^3)	1.810	1.666	1.808
μ(MoKα) (cm^{-1})	38.82	28.89	32.86
refs total	41493	79825	38003
refs unique ($I > 2.00\sigma(I)$)	19873 (16373)	18048 (13254)	19843 (13004)
R_{int}	0.0388	0.0941	0.1024
R_1 ($I > 2.00\sigma(I)$)	0.0888	0.0840	0.1190
wR_2 (all reflections)	0.3425	0.2733	0.3677

the successful structure reported here. PLATON/ADDSYM[26] does not suggest a change in space group while PLATON/SPGRfromEX[26] also agrees with the use of space group $P1$. A total of 415 electrons per unit cell were recovered in one void (total volume 2224 Å^3); that is 207.5 electrons per formula unit. Diffuse electron density was present prior to the application of SQUEEZE, and was assigned as 20 lattice solvent H_2O molecules per formula unit. Similarity and isotropic restraints were applied to several of the terminal ligand ring carbon and nitrogen atoms.

For all structures treated by SQUEEZE, the calculated lattice solvent content has been included in the formula for the calculation of intensive properties.

Variable temperature direct current (DC) and alternating current (AC) magnetic measurements were carried out with a Quantum Design MPMS5S SQUID magnetometer (0−5 T), with diamagnetic corrections applied using Pascal's constants, and appropriate corrections for sample holders used. Elemental analyses were carried out by Canadian Microanalytical, Delta, BC. The complexes are listed with the formulas based on the structural analysis, and may differ from those obtained through elemental analysis carried out on bulk samples. Infrared spectral data were obtained with a Bruker Alpha-P Diamond ATR spectrometer.

Synthesis of Complexes. *[(L4-2H)$_4$Gd$_4$(CH$_3$O)$_4$](CH$_3$CN)$_6$(CH$_3$OH)$_6$ (1).* $Gd(NO_3)_3{\cdot}6H_2O$ (0.11 g, 0.26 mmol) was dissolved in a mixture of methanol (5 mL) and acetonitrile(10 mL). L4 (0.10 g; 0.24 mmol) was added to the resulting clear colorless solution, triethylamine (0.020 g, 0.20 mmol) was added dropwise, and the reaction mixture was stirred for 45 min. The resulting red solution was gravity filtered and crystallization induced by diffusion with diethyl ether resulting in dark red crystals (21.8 mg, 15% yield) after 4 days. The red crystals were studied by single crystal X-ray diffraction. Elemental analysis calcd. (%) for $[(C_{23}H_{16}N_8O)_4Gd_4(OCH_3)_4](H_2O)_{34}$ $(CH_3CN)_5$: C 39.10, H 4.89, N 15.93; found: C 38.98, H 3.98, N 16.28; Selected IR data (cm^{-1}): 3333(ν_{O-H}), 1646 ($\nu_{C=O}$).

[(L3-2H)$_2$(L3-H)$_2$Gd$_4$(O)(N$_3$)$_4$](CH$_3$CN)$_2$(H$_2$O)$_{21}$ (2). $GdCl_3{\cdot}6H_2O$ (0.050 g, 0.19 mmol) was dissolved in a mixture of methanol (5 mL) and acetonitrile (10 mL). L3 (0.050 g; 0.17 mmol) was added, followed by NaN_3 (0.030 g, 0.46 mmol), with the formation of a red solution which was stirred for 4 h. The solution was then gravity filtered and allowed to crystallize by slow evaporation at room temperature

dx.doi.org/10.1021/ic4008813 | Inorg. Chem. 2013, 52, 6731−6742

resulting in dark red crystals suitable for structural study (77 mg, 62% yield). Elemental analysis calcd. (%) for $[(C_{13}H_{12}N_8O)_2(C_{13}H_{13}N_8O)_2Gd_4(O)(N_3)_4](H_2O)_{25}$: C 25.49, H 4.11, N 25.15; found: C 25.35, H 2.91, N 25.50; Selected IR data (cm^{-1}): 2072, 2017(ν_{N-N}), 1606, 1566 ($\nu_{C=N}$).

[(L2-H)$_3$(L2)Dy$_4$(N$_3$)$_4$(O)]Cl$_3$(H$_2$O)$_3$(CH$_3$CN)$_{1.5}$ ***(3)***. $DyCl_3 \cdot 6H_2O$ (0.10 g, 0.24 mmol) was dissolved in a mixture of methanol (5 mL) and acetonitrile (10 mL), followed by the addition of L2 (0.070 g; 0.26 mmol). NaN_3 (0.020 g, 0.31 mmol) was added, and the reaction mixture was stirred for 45 min at room temperature forming a deep red colored solution. The resulting red solution was gravity filtered and kept at room temperature. Crystallization was induced by diffusion with diethyl ether resulting in dark red crystals (32 mg, 25% yield) after several days suitable for structural analysis. Elemental analysis calcd. (%) for $[(C_{13}H_{11}N_6O)_3(C_{13}H_{12}N_6O)Dy_4(N_3)_4(O)]Cl_3(CH_3OH)_3(H_2O)_{19}$: C 26.97, H 3.91, N 20.59; found: C 27.02, H 2.81, N 20.48. Selected IR data (cm^{-1}): 2070, 2020(ν_{N-N}), 1650 ($\nu_{C=N}$).

[(L3-2H)$_2$(L3-H)$_2$(L3)$_2$Dy$_4$(OH)$_4$]Cl$_2$(H$_2$O)$_{20}$ ***(4)***. $DyCl_3 \cdot 6H_2O$ (0.060 g, 0.16 mmol) was dissolved in 10 mL of 2:1 acetonitrile:methanol. L3 (0.040 g; 0.13 mmol) was added, followed by triethylamine (0.020 g, 0.20 mmol), which was added dropwise, and the reaction mixture was stirred for 45 min. The resulting red solution was gravity filtered and allowed to crystallize by slow evaporation resulting in dark red crystals (5.8 mg, 5.0% yield) after 1 day. The red crystals were studied by single crystal X-ray diffraction. Elemental analysis calcd. (%) for $[(C_{13}H_{12}N_8O)_2(C_{13}H_{13}N_8O)_2(C_{13}H_{14}N_8O)_2\ Dy_4(OH)_4]Cl_2(CH_3OH)_5(H_2O)_{26}$: C 31.14, H 4.84, N 21.00; found: C 31.37, H 4.50, N 21.06; Selected IR data (cm^{-1}): 3379 (ν_{O-H}), 3212(ν_{N-H}), 1698 ($\nu_{C=O}$), 1610, 1563 ($\nu_{C=N}$).

[(L3-2H)$_4$(L3)Yb$_4$(OH)$_4$](CH$_3$CN)$_2$(H$_2$O)$_{19}$ ***(5)***. $Yb(NO_3)_3 \cdot 5H_2O$ (0.070 g, 0.16 mmol) was dissolved in 15 mL of 2:1 acetonitrile: methanol, L3 (0.050 g; 0.17 mmol) was added forming a cloudy yellow solution. Triethylamine (0.020 g, 0.20 mmol) was added dropwise, and the reaction mixture was stirred with gentle heating for 35 h. The resulting red solution was gravity filtered and allowed to crystallize by slow evaporation resulting in dark red crystals (35 mg, 40% yield), suitable for single crystal X-ray diffraction. Elemental analysis calcd. (%) for $[(C_{13}H_{12}N_8O)_4(C_{13}H_{14}N_8O)Yb_4(OH)_4](H_2O)_{15}(CH_3CN)$: C 31.50, H 3.91, N 22.48; found: C 31.23,H 3.18, N 22.65; Selected IR data (cm^{-1}): 3403 (ν_{O-H}), 3268 (ν_{N-H}), 1608 ($\nu_{C=N}$).

[(L1-2H)$_2$(L1-H)$_2$Eu$_4$(O)(N$_3$)$_4$](H$_2$O)$_{13}$ ***(6)***. $Eu(NO_3)_3 \cdot 5H_2O$ (0.070 g, 0.16 mmol) was dissolved in 10 mL of 2:1 acetonitrile:methanol, L1 (0.060 g; 0.17 mmol) was added forming a cloudy yellow solution. NaN_3 (0.010 g, 0.16 mmol) was added forming a darker yellow reaction mixture, which was heated gently for 4 h. Triethylamine (0.070 g, 0.70 mmol) was added dropwise and heating continued for 2 h. The resulting orange/red solution was filtered and allowed to crystallize by slow evaporation. Red-orange crystals formed, suitable for structural determination (30 mg, 33% yield). Elemental analyses were carried out on several samples of **6**, but unexpectedly high levels of % N were always obtained. Close inspection of several samples revealed white flecks indicative of the presence of NaN_3, which could not be separated easily either physically or by means of recrystallization. The CHN data suggests the presence of approximately two NaN_3 equivalents per grid in the bulk sample. Magnetic data are not directly affected by the presence of these diamagnetic impurities.

[(L3-2H)$_4$(L3)Ho$_4$(OH)$_4$](H$_2$O)$_{26}$ ***(7)***. $Ho(NO_3)_3 \cdot 5H_2O$ (0.070 g, 0.16 mmol) was dissolved in 10 mL of 2:1 acentonitrile:methanol. L3 (0.060 g; 0.20 mmol) was added, followed by triethylamine (0.020 g, 0.20 mmol), added dropwise, and the reaction was stirred for 3 h. The resulting red solution was gravity filtered and allowed to crystallize by slow evaporation resulting in dark red crystals (18.1 mg, 24% yield), suitable for single crystal X-ray diffraction. Elemental analysis calcd. (%) for $[(C_{13}H_{12}N_8O)_4(C_{13}H_{14}N_8O)Ho_4(OH)_4](H_2O)_{24}$: C 29.53, H 4.34, N 21.19; found: C 29.10, 2.98, N 21.47; Selected IR data (cm^{-1}): 3403 (ν_{O-H}), 3268 (ν_{N-H}), 1608, 1566 ($\nu_{C=O}$),

Description of the Structures. The ligands nominally have two ionizable protons, and their role is not only to provide a scaffold for metal ion coordination, but also an overall charge balance. In most cases two protons are lost per ligand creating L^{2-}, but in some cases partial proton loss occurs, in keeping with the presence of non-coordinating anions, for example, Cl^- (vide infra).

[(L4-2H)$_4$Gd$_4$(CH$_3$O)$_4$](CH$_3$CN)$_6$(CH$_3$OH)$_6$ ***(1)***. The structure of the square Gd_4 [2 × 2] grid **1** is shown in Figure 1a, with a core representation

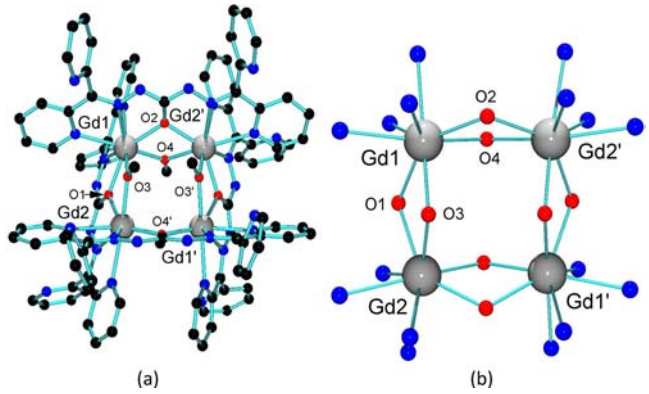

Figure 1. Structural representation of **1** (a) and the grid core (b).

in Figure 1b. Crystal data are given in Table 1, and important distances and angles in Table 2. Each ligand behaves in a similar manner binding one Gd(III) ion in each N_2O pocket, with the four Gd(III) ions bridged by the deprotonated hydrazone oxygen atoms, and also exogenous bridging methoxide, scavenged from the solvent. Each Gd(III) ion is eight-coordinate, with a shape that is best described as square antiprismatic. Gd−Gd separations are quite short (3.775(2) Å, 3.786(2) Å), with Gd−O_{hyd}−Gd angles of 108.5(3) °, 109.1(3) ° and Gd−O_{Me}−Gd angles of 112.3(3) ° and 110.5(3) °. The four ligands are arranged in two pairs above and below the square plane of the four Gd(III) ions, and are canted slightly away from each other. The nonbonded pyridine rings twist relative to the ligands, and are not involved in bonding the Gd(III) ions.

Table 2. Important Distances (Å) and Angles (deg) for 1[a]

Gd1	O3	2.275(7)	
Gd1	O4	2.289(6)	
Gd1	O2	2.320(6)	
Gd1	O1	2.335(7)	
Gd1	N9	2.535(9)	
Gd1	N1	2.540(9)	
Gd1	N10	2.540(8)	
Gd1	N2	2.543(8)	
Gd1	Gd2^i	3.775(2)	
Gd1	Gd2	3.786(2)	
Gd2	O3	2.283(7)	
Gd2	O4^i	2.304(6)	
Gd2	O2^i	2.315(7)	
Gd2	O1	2.332(7)	
Gd2	N13^i	2.536(8)	
Gd2	N6	2.546(10)	
Gd2	N14^i	2.561(8)	
Gd2	N5	2.574(8)	
Gd2	Gd1^i	3.775(2)	
Gd2	O1	Gd1	108.5(3)
Gd2^i	O2	Gd1	109.1(3)
Gd1	O3	Gd2	112.3(3)
Gd1	O4	Gd2^i	110.5(3)

[a]Symmetry operation (i) = 2−*x*, *y*, 1/2−*z*.

[(L3-2H)$_2$(L3-H)$_2$Gd$_4$(O)(N$_3$)$_4$](CH$_3$CN)$_2$(H$_2$O)$_{21}$ ***(2)***. The structure of the square Gd_4 [2 × 2] grid in **2** is shown in Figure 2a, with a core representation in Figure 2b. Crystal data are given in Table 1, and

dx.doi.org/10.1021/ic4008813 | Inorg. Chem. 2013, 52, 6731−6742

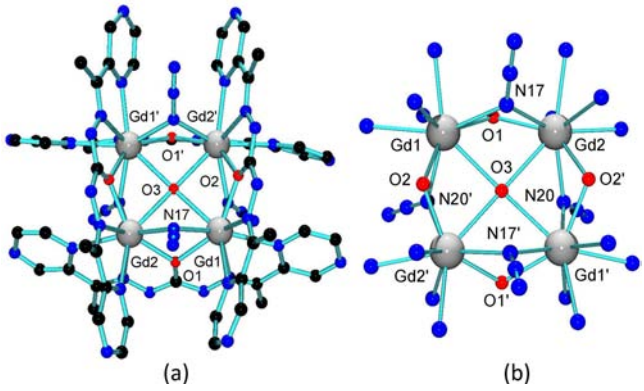

Figure 2. Structural representation of **2** (a) and the grid core (b).

important distances and angles in Table 3. Each ligand binds two Gd(III) ions in the usual manner, with the four metal ions arranged

Table 3. Important Distances (Å) and Angles (deg) for 2[a]

Gd1	O2	2.308(4)	
Gd1	O1	2.341(4)	
Gd1	N20^{i}	2.473(5)	
Gd1	N17	2.479(5)	
Gd1	N11	2.509(5)	
Gd1	N9	2.521(5)	
Gd1	N3	2.565(5)	
Gd1	N1	2.570(5)	
Gd1	O3	2.6084(7)	
Gd1	Gd2^{i}	3.6706(10)	
Gd1	Gd2	3.7040(9)	
Gd2	O2^{i}	2.298(4)	
Gd2	O1	2.337(4)	
Gd2	N17	2.456(5)	
Gd2	N20	2.508(5)	
Gd2	N14^{i}	2.533(5)	
Gd2	N6	2.536(5)	
Gd2	N8	2.543(5)	
Gd2	N16^{i}	2.556(5)	
Gd2	O3	2.6087(6)	
Gd2	Gd1^{i}	3.6706(9)	
Gd2	O1	Gd1	104.71(17)
Gd2^{i}	O2	Gd1	105.68(17)
Gd1	O3	Gd1^{i}	174.4(3)
Gd1	O3	Gd2	90.47(2)
Gd1	O3	Gd2	89.43(2)
Gd2	O3	Gd2^{i}	177.8(3)
Gd2	N17	Gd1	97.28(19)
Gd1^{i}	N20	Gd2	94.95(17)

[a]Symmetry operation (i) = x, 3/2−y, 1/2−z.

in a [2 × 2] square grid structural arrangement, bridged by four deprotonated hydrazone oxygen atoms. In addition four μ_2-1,1-azide bridges also link adjacent Gd(III) ions along the sides of the square, and for the first time with Gd(III) a μ_4-oxide appears in the middle of the square, bound in an almost flat geometry. Each Gd(III) ion is nine-coordinate, with a shape that is best described as a square antiprism with an additional donor on one pseudosquare face. Gd−Gd distances are quite short falling in the range 3.67−3.71 Å. Gd−O distances fall in the range 2.29−2.61 Å, with longer distances to the μ_4 oxide O3. Dy−N distances fall in the range 2.47−2.57 Å with the shortest distances involving the μ_2-1,1-azide bridges. The averaged Gd−O_{hyd}−Gd bridge angles are 105.2°, while the Gd−O3−Gd angles involving the μ_4 oxide are close to 90° (89.43(2)°, 90.47(2) °). The Gd_4 square is almost planar, with O3 being displaced very slightly from the least-squares plane by 0.091(7) Å toward the two N17 azide bridges.

[(L2-H)3(L2)$Dy_4(N_3)_4$(O)]$Cl_3(H_2O)_3(CH_3CN)_{1.5}$ (**3**). The structure of the square Dy_4 [2 × 2] grid is shown in Figure 3a, with a core

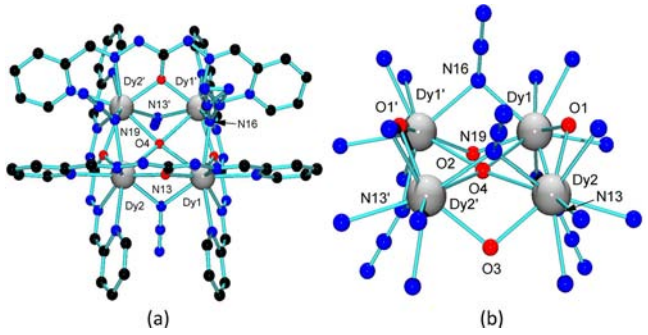

Figure 3. Structural representation of **3** (a) and the grid core (b).

representation in Figure 3b. Crystal data are given in Table 1, and important distances and angles in Table 4. Each ligand binds two Dy(III)

Table 4. Important Distances (Å) and Angles (deg) for 3[a]

Dy1	O1	2.292(4)	
Dy1	O2	2.300(3)	
Dy1	N16	2.427(4)	
Dy1	N13	2.476(4)	
Dy1	N2	2.491(4)	
Dy1	N8	2.498(4)	
Dy1	N1	2.539(5)	
Dy1	N7	2.561(5)	
Dy1	O4	2.684(4)	
Dy1	Dy1^{i}	3.6951(11)	
Dy1	Dy2	3.7062(9)	
Dy2	O1	2.306(4)	
Dy2	O3	2.316(3)	
Dy2	N19	2.450(4)	
Dy2	N13	2.485(4)	
Dy2	N11	2.497(4)	
Dy2	N5	2.522(4)	
Dy2	N10	2.541(4)	
Dy2	O4	2.556(4)	
Dy2	N6	2.562(5)	
Dy2	Dy2^{i}	3.6561(11)	
Dy1	O1	Dy2	107.43(14)
Dy1^{i}	O2	Dy1	106.91(19)
Dy2	O3	Dy2^{i}	104.24(17)
Dy2^{i}	O4	Dy2	91.30(18)
Dy2^{i}	O4	Dy1	169.7(2)
Dy2	O4	Dy1	89.98(3)
Dy2 ^{i}	O4	Dy1^{i}	89.98(3)
Dy2	O4	Dy1^{i}	169.7(2)
Dy1	O4	Dy1^{i}	86.98(16)
Dy1	N13	Dy2	96.66(14)
Dy1	N16	Dy1^{i}	99.2(2)
Dy2^{i}	N19	Dy2	96.5(2)

[a]Symmetry operation (i) = 1−x, y, z.

ions as in **2** with the four Dy(III) ions arranged again in a [2 × 2] square grid structure, bridged by four deprotonated hydrazone oxygen atoms. Four μ_2-1,1-azide bridges again link the metal ions along the square edges, and as in **2**, a μ_4 oxide appears in the middle of the Dy_4 square, bound in an almost flat geometry. Each Dy(III) ions is

dx.doi.org/10.1021/ic4008813 | Inorg. Chem. 2013, 52, 6731−6742

nine-coordinate, with a shape that is best described as a square antiprism with an additional donor on one pseudosquare face. Dy−Dy distances are quite short falling in the range 3.65−3.71 Å. Dy−O distances fall in the range 2.29−2.69 Å, with longer distances to the μ_4 oxide O4 (2.55−2.69 Å). Dy−N distances fall in the range 2.42−2.57 Å with the shortest distances involving the μ_2-1,1-azide bridges. Dy−O_{hyd}−Dy bridge angles fall in the range 104.2−107.5°, while the Dy−O4−Dy angles involving the μ_4 oxide fall in the range 86.9−91.3°, close to 90°. The Dy_4 square is planar, and O4 is displaced very slightly from the plane by 0.229(7) Å toward the two N13 azide bridges.

[(L3-2H)$_2$(L3-H)$_2$(L3)$_2$Dy$_4$(OH)$_4$]Cl$_2$(H$_2$O)$_{20}$ ***(4)***. There are two independent [2 × 2] grids in the asymmetric unit, with each one having two extra, loosely associated, uncomplexed ligands present. The structure of one of the square Dy_4 [2 × 2] grids is shown in Figure 4a, with

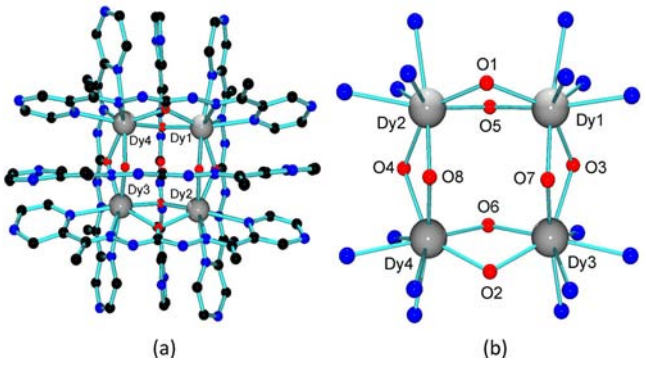

Figure 4. Structural representation of **4** (a) and the grid core (b).

a core representation in Figure 4b (the other grid is essentially the same). Crystal data are given in Table 1, and important distances and angles in Table 5. Each ligand binds two Dy(III) ions in the usual manner, with the four Dy(III) ions arranged in a [2 × 2] square grid structure, bridged by four deprotonated hydrazone oxygen atoms. OH groups are present as extra bridges, leading to eight-coordinate coordination environments at each Dy center, with geometries close to square-antiprismatic. The extra ligands are symmetrically disposed in between pairs of complexed ligands, with short contacts between the hydrazone oxygen atoms and the internal OH bridges (O−O contacts 2.77−2.81 Å) (Figure 5). The contacts are the only direct pseudobonding interactions holding the ligands in place. The short C−O distances (1.19−1.26 Å) indicate ketonic groups at the CO functions. However, the extra ligands appear not to be involved in any direct π-type interactions with neighboring ligands, because of the aromatic rings being offset, but some short atom−atom contacts are <3.3 Å, implying that in addition to the H-bonding contacts, which are clearly tethering the ligands to the grid, there may also be longer distance electrostatic interactions contributing to the stability of the structural arrangement. Dy−$O_{hydrazone}$−Dy angles fall in the range 106.2−108.9°, and Dy−OH−Dy angles in the range 111.4−114.5°. Dy−Dy distances fall in the range 3.75−3.77 Å.

Two additional chloride ions appear in the structure per grid subunit, suggesting that some ligands within the grid may not be fully deprotonated. An alternative possibility could be that the extra ligands are protonated in order for a charge balance. However, despite the good structural refinement, it was not possible to locate protons on the free ligands, or to identify pronated nitrogen sites on the complexed ligands. The formula (vide supra) assumes the former case.

[(L3-2H)$_4$(L3)Yb$_4$(OH)$_4$](CH$_3$CN)$_2$(H$_2$O)$_{19}$ ***(5)***. The structure of the square [2 × 2] Yb_4 grid is shown in Figure 6a and a core structure in Figure 6b. Crystal data are given in Table 1, and important distances and angles in Table 6. The grid has the usual arrangement of four ligands and four metals, with additional OH bridges linking the Yb(III) ions within the square. There is one extra ligand in **5** (rather than two in **4**), positioned in between two coordinated ligands. However the extra ligand is closer to one coordinated ligand than the other, and parallel with it, partly because the two coordinated ligands are not parallel themselves. The extra ligand is locked in place by hydrogen bonds between O5 and two coordinated hydroxides (O8, O9; 2.913(8) and 2.831(9) Å, respectively) (Figures 6a,b), and also by π contacts to the parallel ligand (for the rings containing N9 and N10 to N33 and N34, the centroid to centroid separation is 3.669(8) Å, offset by 1.32(2) Å, with a plane−plane angle of 13.0(4)°; for the rings containing N15 and N16 to N39 and N40, these measurements are 3.812(7) Å, 1.950(15) Å and 8.6(4)°, respectively. Yb−O distances fall in the range 2.18−2.33 Å, and Yb−N distances in the range 2.44−2.58 Å. Yb−OH−Yb angles fall in the range 111.8−109.7°, and Yb−$O_{hydrazone}$−Yb angles fall in the range 105.1−109.7°. Yb−Yb distances are quite short (3.675 Å ave.). Each Yb ion is eight-coordinate with geometries approximating square-antiprismatic.

[(L1-2H)$_2$(L1-H)$_2$Eu$_4$(O)(N$_3$)$_4$](H$_2$O)$_{13}$ ***(6)***. The structure of the square [2 × 2] Eu_4 grid is shown in Figure 7a and a core structure in Figure 7b. Crystal data are given in Table 1, and important distances and angles in Table 7. The grid has the typical arrangement of four ligands and four metals, with additional N_3^- bridges linking the Eu(III) ions within the square, and the commonly observed central μ_4-O oxide. Eu−O distances fall in the range 2.30−2.70 Å, with longer distances to the central μ_4-O5, and Eu−N distances fall in the range 2.52−2.67 Å. Eu−$O_{hydrazone}$−Eu angles fall in the range 106.0−108.2°, Eu−N−Eu angles fall in the range 93.2−96.7°, and angles to the central oxide O5 are close to 90° (89.0−96.7°; angle sum 359.8°), indicating an essentially square Eu_4O subunit. The average Eu−Eu distance is 3.761(2) Å. Each Eu(III) ions is nine-coordinate, with a shape that is best described as a square antiprism with an additional N donor on one pseudosquare face.

[(L3-2H)$_4$(L3)Ho$_4$(OH)$_4$](H$_2$O)$_{26}$ ***(7)***. The structure of the square [2 × 2] Ho_4 grid reveals that there is one extra ligand bound to the grid, rather than two as is the case for **4**. The grid cation minus the extra ligand is shown in Figure 8 a, and a projection showing the unusual orientation of the extra ligand in Figure 8 b. Crystal data are given in Table 1, and important distances and angles in Table 8. In the present case the extra ligand is tethered to the grid via two H-bonding contacts from O9 to O5 and O6 (2.84−2.91 Å), but is not oriented symmetrically between the two adjacent ligands. It lies closer to the ligand which bridges Ho1 and Ho3, and the two ligands are almost eclipsed with a slight misalignnment of the terminal pyrazine rings. Least squares analysis of the terminal pyrazine rings containing N23 and N24 to N39 and N40 gave the centroid to centroid separation of 3.767(9) Å, offset by 1.35(2) Å, with a plane−plane angle of 9.9(5)°; for the rings containing N17 and N18 to N33 and N34, these measurements are 3.677(10) Å, 1.32(2) Å, and 10.3(5)°, respectively. This indicates that the preferred asymmetric arrangement of the extra ligand results through additional π interactions between the ligands. It is of interest to compare the average Ho−Ho distance (3.716 Å), with the Dy−Dy distance in **4** (3.757 Å), which appears to reflect the smaller size of Ho(III). This small difference may be critical in terms of the apparent preference of the symmetric disposition of the extra ligands in **4**, and the asymmetric disposition of the single extra ligand in **7**. The average Ho−OH−Ho angle (112.1°) and the average Ho−$O_{hydrazone}$−Ho angle (107.9°) are comparable with those in **4** (112.9°, 107.3° respectively).

Self-Assembly in the Lanthanide Group. The recent discovery that simple ditopic hydrazone based ligands (e.g., L1) can organize four Ln(III) ions (Ln = Dy, Tb) into a pseudosquare [2 × 2] grid arrangements,[16] using construction principles which have been generally applicable to the transition elements, represents a major step forward in the quest for designer complexes of the lanthanides despite their large ionic radii and coordination numbers, which typically exceed six and often exceed eight. This was assumed to be a limiting constraint with the lanthanides, but clearly is not, as has been demonstrated (vide supra) and paves the way for future endeavors into larger grid based systems with more complex ligands. Ionic radii for the Ln(III) series gradually decrease from 101 pm (Ce(III)) to 86.1 pm (Lu(III)), approaching the ionic radii typical of transition metal ions in the +2 oxidation state (86−74 pm for Ti to Zn). In the present and previous study,[16] the [2 × 2] grid examples include the elements Eu, Gd, Tb, Dy, Ho, and Yb, which cluster to the right side of the

dx.doi.org/10.1021/ic4008813 | Inorg. Chem. 2013, 52, 6731−6742

Table 5. Important Distances (Å) and Angles (deg) for 4

Dy1	O7	2.229(6)	Dy5	Dy6	3.7560(7)		
Dy1	O5	2.267(6)	Dy5	Dy7	3.7569(8)		
Dy1	O3	2.319(7)	Dy6	O18	2.212(7)		
Dy1	O1	2.356(6)	Dy6	O15	2.260(7)		
Dy1	N1	2.547(8)	Dy6	O14	2.313(7)		
Dy1	N3	2.548(9)	Dy6	O11	2.322(6)		
Dy1	N19	2.593(9)	Dy6	N54	2.502(8)		
Dy1	N17	2.601(10)	Dy6	N56	2.533(9)		
Dy1	Dy2	3.7544(7)	Dy6	N75	2.555(9)		
Dy1	Dy3	3.7558(8)	Dy6	N73	2.609(9)		
Dy2	O8	2.206(7)	Dy6	Dy8	3.7618(8)		
Dy2	O5	2.275(6)	Dy7	O17	2.259(6)		
Dy2	O1	2.285(6)	Dy7	O16	2.298(6)		
Dy2	O4	2.342(6)	Dy7	O12	2.321(7)		
Dy2	N6	2.496(9)	Dy7	O13	2.369(7)		
Dy2	N8	2.577(8)	Dy7	N59	2.483(9)		
Dy2	N25	2.597(9)	Dy7	N57	2.532(8)		
Dy2	N27	2.604(9)	Dy7	N72	2.538(9)		
Dy2	Dy4	3.7611(8)	Dy7	N70	2.556(8)		
Dy3	O7	2.239(6)	Dy7	Dy8	3.7567(7)		
Dy3	O6	2.273(6)	Dy8	O16	2.240(6)		
Dy3	O2	2.319(7)	Dy8	O18	2.268(7)		
Dy3	O3	2.378(7)	Dy8	O12	2.307(6)		
Dy3	N11	2.499(9)	Dy8	O14	2.388(7)		
Dy3	N9	2.528(10)	Dy8	N62	2.477(9)		
Dy3	N22	2.532(9)	Dy8	N80	2.506(9)		
Dy3	N24	2.555(9)	Dy8	N64	2.538(9)		
Dy3	Dy4	3.7571(7)	Dy8	N78	2.556(9)		
Dy4	O6	2.275(7)	Dy2	O1	Dy1	108.0(3)	
Dy4	O8	2.278(6)	Dy4	O2	Dy3	108.9(3)	
Dy4	O2	2.300(6)	Dy1	O3	Dy3	106.2(3)	
Dy4	O4	2.362(7)	Dy2	O4	Dy4	106.2(2)	
Dy4	N14	2.500(9)	Dy1	O5	Dy2	111.5(3)	
Dy4	N32	2.531(10)	Dy3	O6	Dy4	111.4(3)	
Dy4	N30	2.544(9)	Dy1	O7	Dy3	114.4(3)	
Dy4	N16	2.567(8)	Dy2	O8	Dy4	114.0(3)	
Dy5	O17	2.224(7)	Dy6	O11	Dy5	107.2(2)	
Dy5	O15	2.276(6)	Dy8	O12	Dy7	108.5(3)	
Dy5	O13	2.311(7)	Dy5	O13	Dy7	106.8(2)	
Dy5	O11	2.345(6)	Dy6	O14	Dy8	106.3(2)	
Dy5	N51	2.491(8)	Dy6	O15	Dy5	111.8(3)	
Dy5	N67	2.538(9)	Dy8	O16	Dy7	111.7(3)	
Dy5	N49	2.552(8)	Dy5	O17	Dy7	113.9(3)	
Dy5	N65	2.604(9)	Dy6	O18	Dy8	114.2(3)	

series where ionic radii are smaller. It is of interest to note that with Pr(III) (ionic radius 99 pm) only a dinuclear complex has been produced,[30] and so there may be a limiting Ln(III) ion size which will accommodate a compact grid structure. Further studies with this class of ligands and the remaining lanthanide ions will shed more light on this issue.

The demonstrated application of transition metal grids (e.g., [2 × 2] (Co(II)), [3 × 3], [4 × 4], [5 × 5] (Mn(II))) to surfaces, for example, HOPG, Au,[11,12,28,29] with monolayer arrangements in some cases,[28,29] has shown that at the single molecule level some unique property may possibly be exploitable for, for example, information storage. In the case of the lanthanide grids one possibility would be their SMM character (vide infra).

MAGNETIC PROPERTIES

$[(L4\text{-}2H)_4Gd_4(CH_3O)_4](CH_3CN)_6(CH_3OH)_6$ (1). Variable temperature magnetic data for **1** are shown in Figure 9 as a plot of χT versus temperature. The value at 300 K (31.3 cm^3 mol^{-1} K) compares closely with the expected value for four uncoupled Gd(III) ions ($^8S_{7/2}$, g = 2.0; 31.5 cm^3 mol^{-1} K). The drop in χT on lowering temperature signals antiferromagnetic exchange between the metal ions. The isotropic nature of the Gd(III) ion allows the variable temperature data to be analyzed using a simple Heisenberg expression (eq 1) for the interaction for four S = 7/2 spin centers arranged in a square.

$$H_{ex} = -J\{S_1 \cdot S_2 + S_2 \cdot S_3 + S_3 \cdot S_4 + S_1 \cdot S_4\} \quad (1)$$

A good data fit gave g = 1.99(1), J = −0.095(2) cm^{-1} (10^2R = 0.54; $R = [\Sigma(\chi_{obs} - \chi_{calc})^2/\Sigma\chi_{obs}^2]^{1/2}$). The solid line in Figure 9 was calculated with these parameters. The small value of $|-J|$ is typical for polynuclear Gd(III) complexes.[31,32]

$[(L3\text{-}2H)_2(L3\text{-}H)_2Gd_4(O)(N_3)_4](CH_3CN)_2(H_2O)_{21}$ (2). Variable temperature magnetic data for **2** are shown in Figure 10 as a plot of of χT versus temperature. The value at 300 K (30.8 cm^3 mol^{-1} K) compares closely with the expected value for four

dx.doi.org/10.1021/ic4008813 | Inorg. Chem. 2013, 52, 6731−6742

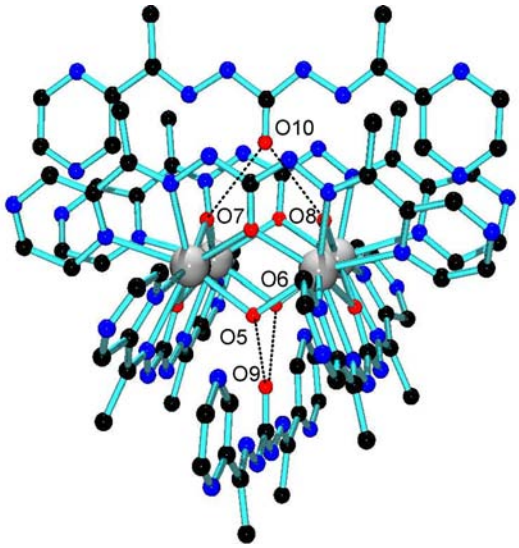

Figure 5. Hydrogen bonding connections between the grid and extra ligands in **4**.

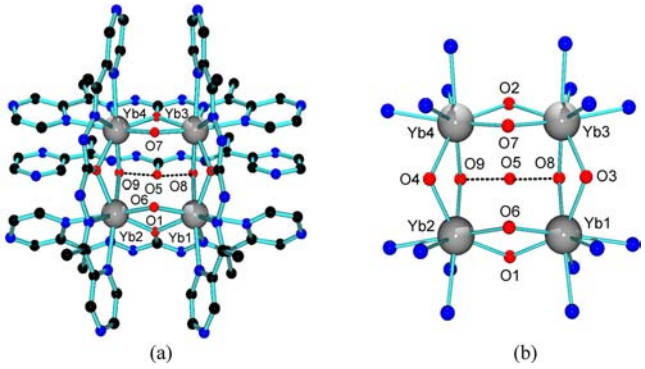

Figure 6. Structural representation of **5** (a) and the grid core (b).

uncoupled Gd(III) ions ($^8S_{7/2}$, g = 2.0; 31.5 cm^3 mol^{-1} K). The drop in χT on lowering temperature again signals antiferromagnetic exchange, and the data were fitted as for **1** to give g = 1.93(1), J = −0.10(2) cm^{-1} (10^2R = 0.71; $R = [\Sigma(\chi_{obs} - \chi_{calc})^2/\Sigma\chi_{obs}^2]^{1/2}$). The solid line in Figure 10 was calculated with these parameters. The small |−J| value is again indicative of weak intramolecular antiferromagnetic exchange, and perhaps the reason it is slightly larger than for **1**, may indicate the effect of the combination of the three differing bridge groups. Using criteria established for transition metal complexes with metal ions, for example, Cu(II) bridged by μ_2-1,1-azide with bridge angles <98°, would possibly suggest ferromagnetic exchange,[33,34] while for the Gd−$O_{hydrazone}$−Gd bridges (Gd−O−Gd 104−106°) antiferromagnetic exchange would be predicted.[35] The case for the unusual central μ_4-O is hard to predict because of a lack of examples. Suffice to say that if ferromagnetic and antiferromagnetic terms are involved the net effect will be a summation. In the present case clearly antiferromagnetic terms dominate overall.

[(L2-H)3(L2)Dy4(N_3)$_4$(O)]$Cl_3(H_2O)_3(CH_3CN)_{1.5}$ (3). Variable temperature DC magnetic data (χT vs T plot) for **3** are shown in Figure 11. The room temperature χT value of 54.2 cm^3 mol^{-1} K is in reasonable agreement with the theoretical value of 56.7 cm^3 K mol^{-1} for four noninteracting Dy(III) ions (S = 5/2, L = 5, $^6H_{15/2}$, g = 4/3). The χT values decrease slowly down to approximately 50 K then more rapidly down to 2.0 K

Table 6. Important Distances (Å) and Angles (deg) for 5

Yb1	O8	2.207(7)	
Yb1	O6	2.220(6)	
Yb1	O1	2.284(5)	
Yb1	O3	2.290(5)	
Yb1	N3	2.472(8)	
Yb1	N19	2.521(8)	
Yb1	N1	2.527(6)	
Yb1	N17	2.561(8)	
Yb1	Yb3	3.6779(10)	
Yb1	Yb2	3.6986(12)	
Yb2	O9	2.223(7)	
Yb2	O1	2.239(6)	
Yb2	O6	2.247(5)	
Yb2	O4	2.294(5)	
Yb2	N8	2.460(7)	
Yb2	N6	2.468(7)	
Yb2	N27	2.529(7)	
Yb2	N25	2.577(7)	
Yb2	Yb4	3.6656(10)	
Yb3	O7	2.189(6)	
Yb3	O8	2.202(5)	
Yb3	O2	2.248(6)	
Yb3	O3	2.308(6)	
Yb3	N9	2.441(8)	
Yb3	N11	2.472(8)	
Yb3	N22	2.494(9)	
Yb3	N24	2.549(8)	
Yb3	Yb4	3.6577(12)	
Yb4	O9	2.201(6)	
Yb4	O7	2.206(5)	
Yb4	O2	2.233(6)	
Yb4	O4	2.324(6)	
Yb4	N30	2.482(8)	
Yb4	N14	2.488(8)	
Yb4	N16	2.507(7)	
Yb4	N32	2.531(8)	
Yb2	O1	Yb1	109.7(2)
Yb4	O2	Yb3	109.4(3)
Yb1	O3	Yb3	106.2(2)
Yb2	O4	Yb4	105.1(2)
Yb1	O6	Yb2	111.8(3)
Yb3	O7	Yb4	112.7(3)
Yb3	O8	Yb1	113.1(3)
Yb4	O9	Yb2	111.9(3)

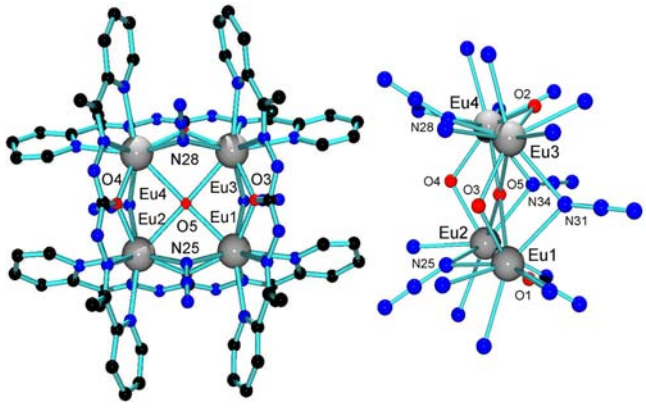

Figure 7. Structural representation of **6** (a) and the grid core (b).

dx.doi.org/10.1021/ic4008813 | Inorg. Chem. 2013, 52, 6731−6742

Table 7. Important Distances (Å) and Angles (deg) for 6

Eu1	O3	2.327(6)	
Eu1	O1	2.355(6)	
Eu1	N31	2.540(8)	
Eu1	N25	2.541(7)	
Eu1	N13	2.555(8)	
Eu1	N14	2.579(8)	
Eu1	N2	2.584(7)	
Eu1	N1	2.593(7)	
Eu1	O5	2.600(6)	
Eu1	C8	3.229(10)	
Eu1	Eu3	3.7291(15)	
Eu1	Eu2	3.7810(13)	
Eu2	O4	2.331(6)	
Eu2	O1	2.348(6)	
Eu2	N25	2.520(7)	
Eu2	N34	2.524(8)	
Eu2	N6	2.551(8)	
Eu2	N5	2.565(8)	
Eu2	N19	2.574(8)	
Eu2	N20	2.593(8)	
Eu2	O5	2.663(7)	
Eu2	Eu4	3.7611(16)	
Eu3	O3	2.309(6)	
Eu3	O2	2.374(5)	
Eu3	N28	2.549(8)	
Eu3	N17	2.551(7)	
Eu3	N8	2.581(8)	
Eu3	N31	2.594(8)	
Eu3	N18	2.600(9)	
Eu3	N7	2.662(8)	
Eu3	O5	2.679(7)	
Eu3	C38	3.265(10)	
Eu3	Eu4	3.7736(13)	
Eu4	O4	2.313(6)	
Eu4	O2	2.351(6)	
Eu4	N28	2.536(8)	
Eu4	N23	2.558(8)	
Eu4	N34	2.562(8)	
Eu4	N24	2.573(8)	
Eu4	N11	2.573(7)	
Eu4	N12	2.597(9)	
Eu4	O5	2.700(6)	
Eu2	O1	Eu1	107.0(2)
Eu4	O2	Eu3	106.0(2)
Eu3	O3	Eu1	107.1(2)
Eu4	O4	Eu2	108.2(2)
Eu1	O5	Eu2	91.8(2)
Eu1	O5	Eu3	89.86(19)
Eu2	O5	Eu3	175.9(3)
Eu1	O5	Eu4	177.6(3)
Eu2	O5	Eu4	89.06(19)
Eu3	O5	Eu4	89.1(2)
Eu2	N25	Eu1	96.7(2)
Eu4	N28	Eu3	95.8(3)
Eu1	N31	Eu3	93.2(3)
Eu2	N34	Eu4	95.4(3)

reaching a value of 5.6 cm^3 K mol^{-1}. Such behavior is typical of single ion Dy(III) properties and not necessarily indicative of any antiferromagnetic exchange. Magnetization plots (M vs H/T) from 2−8 K (Figure 12) at high fields (up to 5 T) and down to 2.0 K show nonsaturation as well as nonsuperposition on a

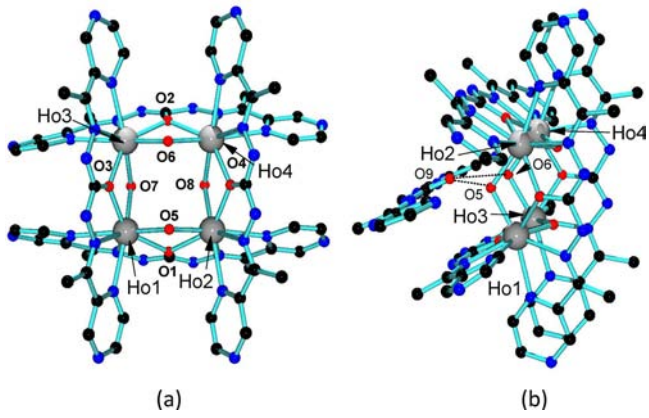

Figure 8. Structural representation of the [2 × 2] grid in **7** (a) and a projection showing the extra ligand (b).

single curve, indicating the presence of magneto-anisotropy and/or low-lying excited states.

In a previous study[16] we found that a closely related [2 × 2] Dy_4 grid complex, $[Dy_4(L1\text{-}2H)_2(L1\text{-}2H)_2(N_3)_4(O)]\cdot 14H_2O$, involving the same combination of μ_2-1,1-azide, μ4-oxide and μ_2-$O_{hydrazone}$ bridges showed SMM character, with two relaxation processes in the 4−25 K temperature range. Given the slight difference in ligand we decided to measure AC magnetic data for **3** in anticipation of similar behavior. AC magnetic data were collected, with the sample immobilized in eicosane to prevent torqueing, in the temperature range 2−35 K, and with frequencies in the range 1500−10 Hz, both at zero DC external bias field and in an optimized DC field of 1800 Oe, to suppress or minimize any quantum based relaxation processes. This was established through monitoring the χ'' response as a function of bias field and frequency until no further change in response was observed. At 0 Oe two frequency dependent peaks were observed in the profiles of both χ' and χ'' as a function of temperature (Supporting Information, Figures S1, S2, respectively). One suite of peaks, appearing in both χ' and χ'', occurred in the range 5−7 K, while a second suite of peaks was found for χ' in the range 18−24 K and for χ'' between 10 and 20 K. At 1800 Oe bias field the low temperature peaks essentially disappeared, but the frequency dependent peaks in both χ' and χ'' remained in the higher temperature regime (Figures 13, 14 respectively). This strongly suggests that the lower temperature relaxation process is dominated by quantum relaxation effects, while in the higher temperature regime thermal relaxation processes are involved. This overall behavior is reminiscent of $[Dy_4(L1\text{-}2H)_2(L1\text{-}2H)_2(N_3)_4(O)]\cdot 14H_2O$,[16] but there is a marked distinction. With **3** the low temperature response observed in zero bias field disappears in the presence of a 1800 Oe field, while in the former case the related low temperature response persists. While the overall structures of the two complexes are essentially the same, the ligands differ, with methyl groups being substituted by hydrogen in **3**. While this may be regarded as a subtle ligand difference, it appears to lead to a marked difference in magnetic behavior.

The Cole−Cole plot for **3** (Supporting Information, Figure S3) indicates one frequency dependent relaxation process in the 10−25 K temperature range. The energy barrier for reversal of magnetization was calculated from the temperature dependent peak positions associated with the out of phase, χ'' response (Figure 14), using a thermally activated Arrhenius model ($\tau = \tau_0 \exp(U_{eff}/kT)$. A good straight line was obtained for the ln

dx.doi.org/10.1021/ic4008813 | Inorg. Chem. 2013, 52, 6731−6742

Table 8. Important Distances (Å) and Angles (deg) for 7

Ho1	O5	2.222(8)	
Ho1	O7	2.239(8)	
Ho1	O3	2.286(7)	
Ho1	O1	2.324(8)	
Ho1	N17	2.513(10)	
Ho1	N19	2.522(11)	
Ho1	N3	2.537(10)	
Ho1	N1	2.547(10)	
Ho1	Ho3	3.706(2)	
Ho1	Ho2	3.718(2)	
Ho2	O5	2.234(6)	
Ho2	O8	2.249(7)	
Ho2	O4	2.273(6)	
Ho2	O1	2.347(8)	
Ho2	N27	2.509(11)	
Ho2	N6	2.537(10)	
Ho2	N25	2.538(9)	
Ho2	N8	2.554(10)	
Ho2	Ho4	3.729(2)	
Ho3	O6	2.211(8)	
Ho3	O7	2.250(8)	
Ho3	O3	2.284(7)	
Ho3	O2	2.299(7)	
Ho3	N24	2.471(10)	
Ho3	N22	2.507(9)	
Ho3	N11	2.540(11)	
Ho3	N9	2.551(9)	
Ho3	Ho4	3.710(2)	
Ho4	O6	2.240(7)	
Ho4	O8	2.280(8)	
Ho4	O4	2.283(7)	
Ho4	O2	2.289(8)	
Ho4	N30	2.493(10)	
Ho4	N32	2.502(9)	
Ho4	N14	2.524(9)	
Ho4	N16	2.560(11)	
Ho1	O1	Ho2	105.5(3)
Ho4	O2	Ho3	108.0(3)
Ho3	O3	Ho1	108.4(3)
Ho2	O4	Ho4	109.8(3)
Ho1	O5	Ho2	113.1(3)
Ho3	O6	Ho4	112.9(3)
Ho1	O7	Ho3	111.3(3)
Ho2	O8	Ho4	110.8(3)

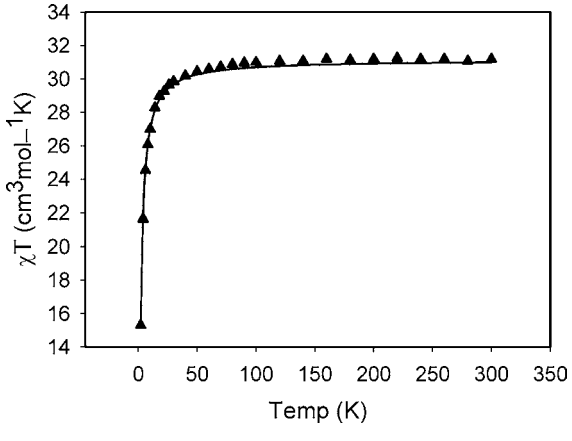

Figure 9. DC magnetic data for **1** (see text for fitted parameters).

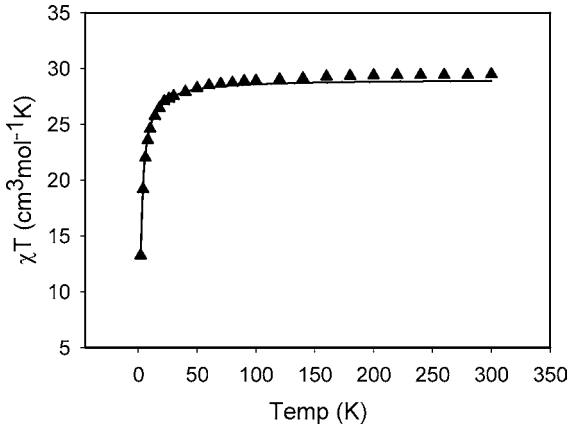

Figure 10. DC magnetic data for **2** (see text for fitted parameters).

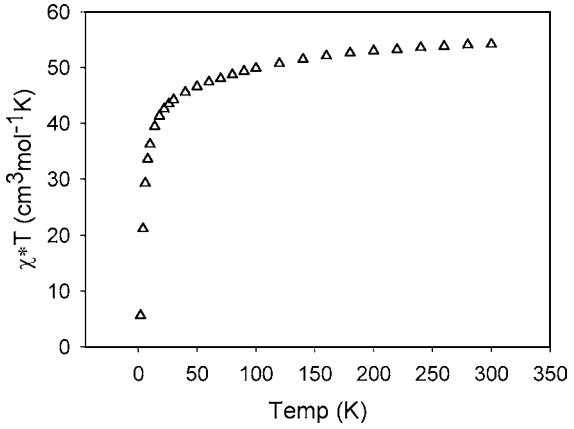

Figure 11. Variable temperature DC magnetic data **3**.

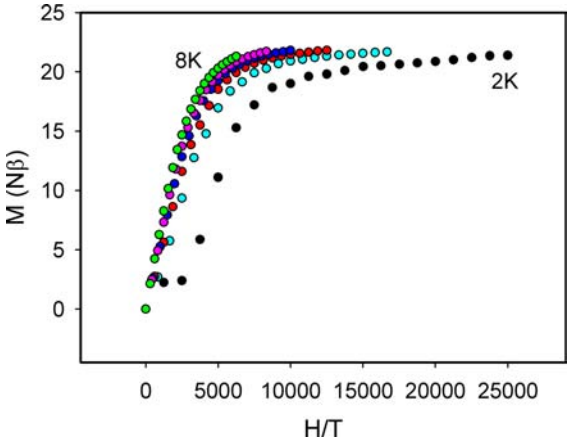

Figure 12. Magnetization vs H/T data for **3**.

τ vs $1/T$ plot (Figure 15), giving $\tau_0 = 6.5(1) \times 10^{-7}$ s and U_{eff} = 110(1) K. This is quite a large energy barrier, but is consistent with the thermal response of the higher temperature (15–25 K) relaxation process observed for $[Dy_4(L1\text{-}2H)_2(L1\text{-}2H)_2(N_3)_4(O)]\cdot 14H_2O$,[16] ($\tau_0 = 4.5 \times 10^{-7}$ s, U_{eff} = 91 K), illustrating the expected similarity. The fact that there is no significant low temperature diversion from the plot indicates that the relaxation process is mostly thermally driven in this temperature regime.

Variable temperature magnetic data for **4** are shown in Figure 16 as a plot of χT vs T, with a room temperature value of 55.1 cm^3 mol^{-1} K, in good agreement with the theoretical value of

dx.doi.org/10.1021/ic4008813 | Inorg. Chem. 2013, 52, 6731–6742

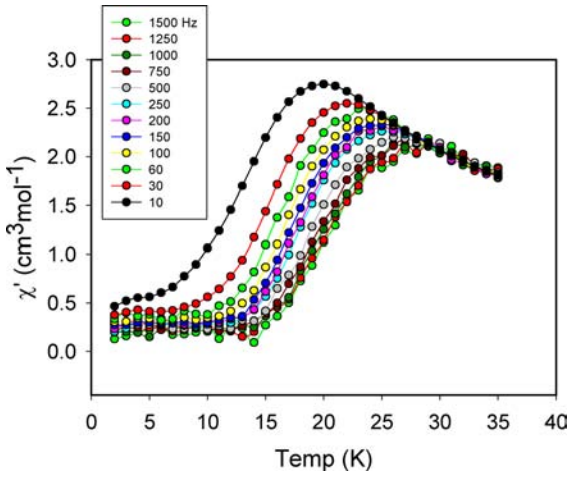

Figure 13. AC (χ') magnetic data for **3** at 1800 Oe external field.

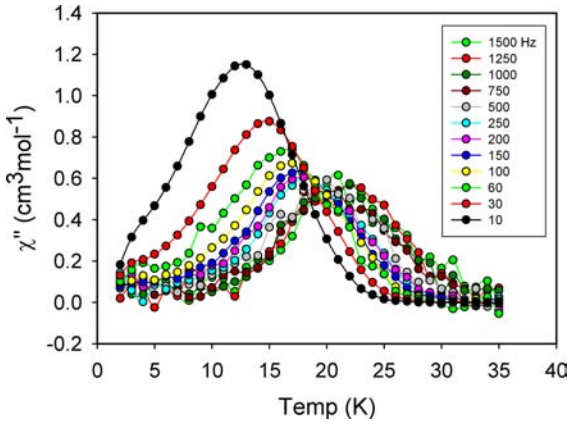

Figure 14. AC (χ'') magnetic data for **3** at 1800 Oe external field.

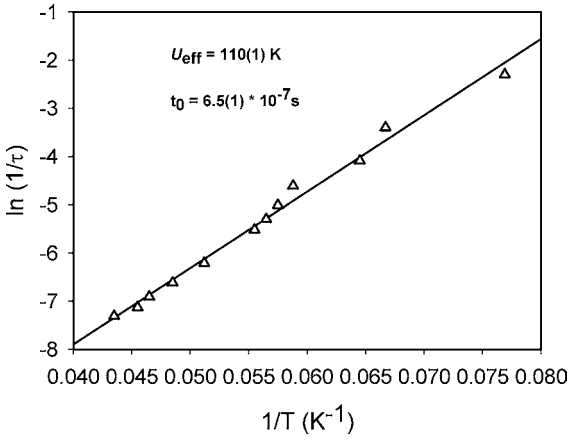

Figure 15. Arrhenius plot for **3** at 1800 Oe external bias field.

56.7 cm^3 mol^{-1} K for four noninteracting Dy(III) ions (S = 5/2, L = 5, $^6H_{15/2}$, g = 4/3), dropping slightly on lowering temperature to ~100 K, then more sharply down to a low value of 32.5 cm^3 mol^{-1} K at 2 K. AC magnetic data show no significant frequency dependent response above 2 K in either χ' or χ'', indicating the absence of SMM character. This behavior is similar to that observed for related [2 × 2] Dy_4 square grids, where the central μ_4-O and μ_2-1,1-azide bridges are absent.[16]

Variable temperature magnetic data for **5** are shown in Figure 16 as a plot of χT vs T, with a room temperature value of

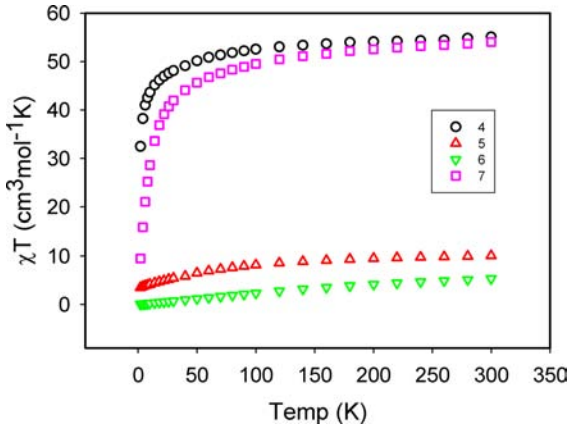

Figure 16. Variable temperature magnetic data for **4**–**7**.

10.1 cm^3 mol^{-1} K, in good agreement with the theoretical value of 10.3 cm^3 mol^{-1} K for four noninteracting Yb(III) ions (S = 1/2, L = 3, $^2F_{7/2}$, g = 4/3), dropping slightly on lowering temperature to ~100 K, then more sharply down to a low value of 5.3 cm^3 mol^{-1} K at 2 K.

Variable temperature magnetic data for **6** are shown in Figure 16 as a plot of χT vs T, with a room temperature value of 5.3 cm^3 mol^{-1} K, in good agreement with the typical values expected four noninteracting Eu(III) ions (S = 6/2, L = 3, $^7F_0$, g = 4/3). χT drops steadily on lowering temperature to a low value of 0.050 cm^3 mol^{-1} K at 2 K, indicating a nonmagnetic ground state, typical of Eu(III).

Variable temperature magnetic data for **7** are shown in Figure 16 as a plot of χT vs T, with a room temperature value of 54.0 cm^3 mol^{-1} K, in good agreement with the typical values expected for four noninteracting Ho(III) ions (S = 4/2, L = 6, $^5I_8$, g = 4/3). χT drops slightly down to ~100 K, then more sharply on lowering temperature to a low value of 9.5 cm^3 mol^{-1} K at 2 K. AC data at variable frequency indicate no dependence in χ' or χ'' above 2 K, indicating the absence of SMM character.

CONCLUSIONS

The self-assembled organization of Ln(III) ions (Ln = Eu, Gd, Dy, Ho, Yb) into square [2 × 2] grid arrays has been achieved using the simple expedient of mixing the Ln(III) salt with a group of ditopic, pentadentate carbohydrazone ligands. The Ln(III) ions are bridged through μ_2-$O_{hydrazone}$ ligand atoms, and depending on the addition of other reagents, μ_2-OMe, μ_4-O, and μ_2-1,1-N_3 bridges also result. The Ln(III) ions adopt eight or nine coordinate geometries, depending on the coligands present, with no labile coordination sites, and all the metal ions appear to be tightly bound within the grid framework. Antiferromagnetic exchange is observed in the Gd(III) examples, while with Dy(III) SMM behavior is observed in special circumstances, when the four Dy(III) ions are bridged internally by μ_4-O, and μ_2-1,1-N_3. Because of the large inherent orbital angular momentum associated with the highly anisotropic Ln(III) ions, intramolecular spin exchange is likely not a deciding factor in determining magnetic properties. However, the polarizing effects of the bridging coligands, for example, μ_4-O, and μ_2-1,1-N_3, which dominate spin properties in the case of the transition metal ions, and the rigid geometry enforced by the primary bis-hydrazone ligands, may be important in the mutual alignment of the easy magnetic axes. The fact that SMM character is absent when, for example, azide and oxide are absent, reinforces this argument.

dx.doi.org/10.1021/ic4008813 | Inorg. Chem. 2013, 52, 6731–6742

■ ASSOCIATED CONTENT

Supporting Information

Further details are given in Figures S1−S3. This material is available free of charge via the Internet at http://pubs.acs.org.

■ AUTHOR INFORMATION

Corresponding Author

*E-mail: lk.thompson@mun.ca.

Notes

The authors declare no competing financial interest.

■ ACKNOWLEDGMENTS

We thank NSERC for financial support for this study, and USRA fellowships for N.M.R. and M.W.D.

■ REFERENCES

(1) Sessoli, R.; Gatteschi, D.; Caneshi, A.; Novak, M. A. *Nature* **1993**, *365*, 141.

(2) (a) Christou, G.; Gatteschi, D.; Hendrickson, D. N.; Sessoli, R. *MRS Bull.* **2000**, *25*, 66. (b) Gatteschi, D.; Sessoli, R. *Angew. Chem., Int.Ed.* **2003**, *42*, 268. (c) Aromi, G.; Brechin, E. K. *Struct. Bonding (Berlin)* **2006**, *122*, 1.

(3) Leuenberger, M. N.; Loss, D. *Nature* **2001**, *410*, 789.

(4) Long, J.; Habib, F.; Lin, P-H; Korobkov, I.; Enright, G.; Ungur, L.; Wernsdorfer, W.; Chibotaru, L. F.; Murugesu, M. *J. Am. Chem. Soc.* **2011**, *133*, 5319.

(5) Tang, J.; Hewitt, I.; Madhu, N. T.; Chastanet, G.; Wernsdorfer, W.; Anson, C. E.; Benelli, C.; Sessoli, R.; Powell, A. K. *Angew. Chem., Int. Ed.* **2006**, *45*, 1729.

(6) Yan, P.-F.; Lin, P.-H.; Habib, F.; Aharen, T.; Murugesu, M.; Deng, Z.-P.; Li, G.-M.; Sun, W.-B. *Inorg. Chem.* **2011**, *50*, 7059.

(7) Lin, P.-H.; Burchell, J. T.; Ungur, L.; Chibotaru, L. F.; Wernsdorfer, W.; Murugesu, M. *Angew. Chem., Int. Ed.* **2009**, *48*, 9489.

(8) Hewitt, I. J.; Tang, J.; Madhu, N. T.; Anson, C. E.; Lan, Y.; Luzon, J.; Etienne, M.; Sessoli, R.; Powell, A. K. *Angew. Chem., Int. Ed.* **2010**, *49*, 6352.

(9) Tian, H.; Guo, Y-N; Zhao, L.; Tang, mJ.; Liu, Z. *Inorg. Chem.* **2011**, *50*, 8688.

(10) Sessoli, R.; Powell, A. K. *Coord. Chem. Rev.* **2009**, *253*, 2328.

(11) Dawe, L. N.; Shuvaev, K. V.; Thompson, L. K. *Chem. Soc. Rev.* **2009**, *38*, 2334.

(12) Milway, V. A.; Abedin, S. M. T.; Niel, V.; Kelly, T. L.; Dawe, L. N.; Dey, S. K.; Thompson, D. W.; Miller, D. O.; Alam, S.; Müller, P.; Thompson, L. K. *Dalton Trans* **2006**, 2835 , and references therein.

(13) Dawe, L. N.; Shuvaev, K. V.; Thompson, L. K. *Inorg. Chem.* **2009**, *48*, 3323.

(14) Anwar, M. U.; Tandon, S. S.; Dawe, L. N.; Habib, F.; Murugesu, M.; Thompson, L. K. *Inorg. Chem.* **2012**, *51*, 1028.

(15) Shuvaev, K. V.; Dawe, L. N.; Thompson, L. K. *Dalton Trans.* **2010**, *39*, 4768.

(16) Anwar, M. U.; Thompson, L. K.; Dawe, L. N.; Habib, F.; Murugesu, M. *Chem. Commun.* **2012**, *48*, 4576.

(17) Sheldrick, G. M. *Acta Crystallogr.* **2008**, *A64*, 112.

(18) Burla, M. C.; Camalli, M.; Carrozzini, B.; Cascarano, G. L.; Giacovazzo, C.; Polidori, G.; Spagna, R. *J. Appl. Crystallogr.* **2003**, *36*, 1103.

(19) Beurskens, P. T.; Admiraal, G.; Beurskens, G.; Bosman, W. P.; de Gelder, R.; Israel, R.; Smits, J. M. M. *DIRDIF99*; The DIRDIF-99 program system, Technical Report of the Crystallography Laboratory; University of Nijmegen: Nijmegen, The Netherlands, 1999.

(20) Cromer, D. T.; Waber, J. T. *International Tables for X-ray Crystallography*; The Kynoch Press: Birmingham, England, 1974; Vol. *IV*, Table 2.2 A.

(21) Ibers, J. A.; Hamilton, W. C. *Acta Crystallogr.* **1964**, *17*, 781.

(22) Creagh, D. C.; McAuley, W. J. *International Tables for X-ray Crystallography*; Wilson, A.J.C., Ed.; Kluwer Academic Publishers: Boston, MA, 1992; Vol *C*Table 4.2.6.8, pp 219−222.

(23) Creagh, D. C.; Hubbell, J. H. *International Tables for X-ray Crystallography*; Wilson, A.J.C., Ed.; Kluwer Academic Publishers: Boston, MA, 1992; Vol *C*, Table 4.2.4.3, pp 200−206.

(24) *CrystalStructure 3.7.0*, Crystal Structure Analysis Package; Rigaku and Rigaku/MSC: The Woodlands TX, 2000−2005.

(25) Watkin, D. J.; Prout, C. K.; Carruthers, J. R.; Betteridge, P. W. *CRYSTALS Issue 10*; Chemical Crystallography Laboratory: Oxford, U.K., 1996.

(26) Spek, A. L. *J. Appl. Crystallogr.* **2003**, *36*, 7.

(27) Petukhov, K.; Alam, M. S.; Rupp, H.; Strömsdorfer, S.; Müller, P.; Scheurer, A.; Saalfrank, R. W.; Kortus, J.; Postnikov, A.; Ruben, M.; Thompson, L. K.; Lehn, J.-M. *Coord. Chem. Rev.* **2009**, *253*, 2387 , and references therein.

(28) Weeks, L.; Thompson, L. K.; Shapter, J. G.; Pope, K. J.; Xu, Z. *J. Microsc.* **2003**, *212*, 102.

(29) Shapter, J. G.; Weeks, L.; Thompson, L. K.; Pope, K. J.; Xu, Z.; Johnston, M. *Proc. SPIE* **2004**, *5275*, 59.

(30) Anwar, M.U.; Shuvaev, K.V.; Thompson, L.K., unpublished results.

(31) John, D.; Rohde, A.; Urland, W. *Z. Naturforsch.* **2006**, *61b*, 699.

(32) Anwar, M. U.; Dawe, L. N.; Tandon, S. S.; Bunge, S. D.; Thompson, L. K. *Dalton Trans.* **2013**, DOI: 10.1039/c3dt32732a.

(33) Tandon, S. S.; Thompson, L. K.; Manuel, M. E.; Bridson, J. N. *Inorg. Chem.* **1994**, *33*, 5555.

(34) Thompson, L. K.; Tandon, S. S.; Manuel, M. R. *Inorg. Chem.* **1995**, *34*, 2356.

(35) Crawford, V. H.; Richardson, H. W.; Wasson, J. R.; Hodgson, D. J.; Hatfield, W. E. *Inorg. Chem.* **1976**, *15*, 2107.